Tissue Segmentation and Partial Volume Estimation with Magnetic Resonance Fingerprinting

Dan Ma[1]; Anagha Deshmane[2]; Debra McGivney[1]; Irene Wang[3]; Chaitra Badve[1]; Vikas Gulani[1]; Mark Griswold[1]

[1]Radiology, Case Western Reserve University, Cleveland, OH, USA
[2]Magnetic Resonance Center, Max Planck Institute for Biological Cybernetics, Tuebingen, Germany
[3]Epilepsy Center, Cleveland Clinic, Cleveland, OH, USA

Introduction

Recent demand for precision medicine and personalized diagnostics has led to increased interest in radiomics and robust quantitative imaging with MRI. To this end, recent technical developments have included anatomical volumetry, quantitative relaxometry, and quantification of tissue microstructural and functional properties such as diffusion and perfusion. Specifically, tissue segmentation has become the basis of quantitative volumetric estimation and volume-based post-processing, which have been used to diagnose and characterize several neurological diseases. For example, multiple sclerosis [1], brain plasticity [2, 3], dementia [4], and epilepsy [5, 6] are associated with global and local brain volume and cortical thickness changes. Anatomical segmentation has also been used to target subcortical structures, such as the subthalamic nucleus (STN) [7], for surgical treatments.

The partial volume (PV) effect is a well-known challenge for any imaging modality with limited image resolution, including MRI, and poses a particular challenge for both quantitative mapping and quantitative image analysis. When the image resolution is lower than the dimension of the anatomical structure, e.g. when image voxels span tissue boundaries, some voxels may contain multiple tissue types. The PV effect causes blurring at these interfaces on the MR images because the contrast or signal of the mixed voxel is a weighted average of that from each single tissue component. For quantitative imaging and image post-processing, the assumption that each voxel contains a single and pure tissue type may lead to mis-classification and thus mask some subtle features or tissue changes, especially at tissue boundaries. Assuming that the signal evolution (for example, a relaxation curve) in each image voxel is characterized by a single tissue property (i.e. T1 or/and T2) may cause errors in tissue property quantification in mixed voxels.

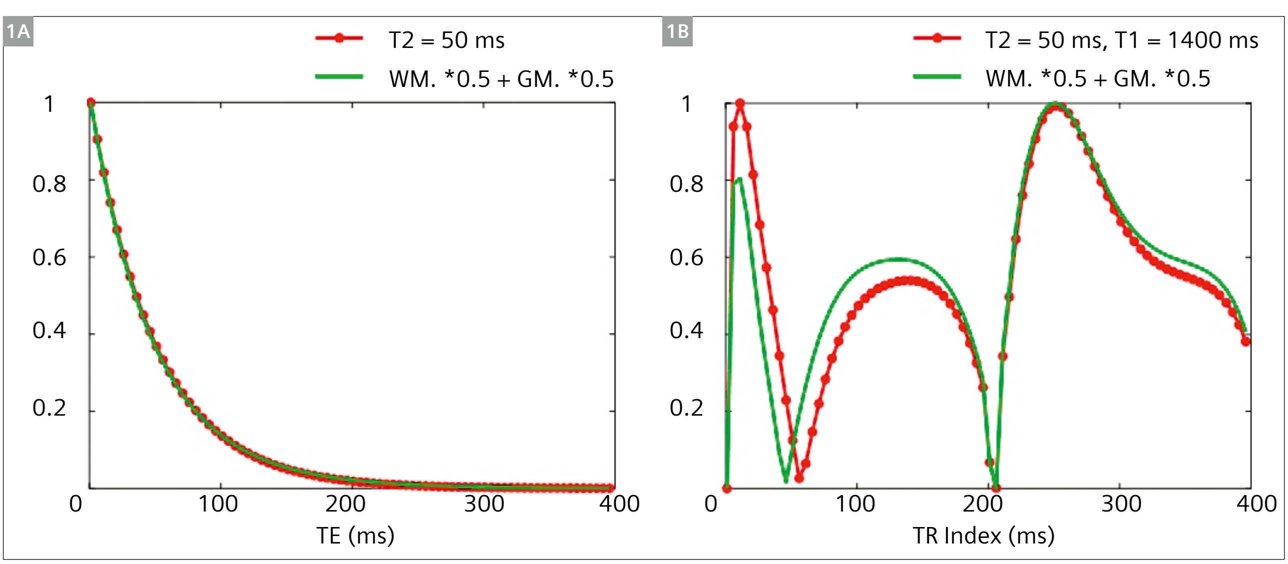

1 Comparison of signal curves from conventional T2 mapping **(1A)** and from MRF **(1B)**. The signal from a PV effect is more distinct from a pure tissue using MRF.

Depending on the desired anatomical scale for analysis of tissue properties within one voxel, certain assumptions about possible voxel compositions can be made. This article concerns multiple tissue components in the slow exchange regime, where no chemical exchange between components is assumed, such that each tissue within a voxel is modeled as a distinct component. Primarily, multi-component models for PV have been used for tissue segmentation, by assuming that each voxel contains mixed signals from pure tissues, such as gray matter (GM), white matter (WM), and CSF for brain tissue segmentation [8–10], or water and fat for fat fraction estimation in the liver [11]. The result of these methods are either hard-threshold tissue classification or soft-threshold tissue fraction maps, which can be further used for tissue volume calculation [6], image feature extraction [12, 13], and disease diagnosis. In addition, multi-component PV models have been used to analyze microstructural features. For example, multiple T2 components have long been considered when analyzing human brain [14], where three components are commonly assumed, including water protons compartmentalized between myelin bilayers, intra- and extracellular water, and free fluid (usually contained in the CSF). The results of the PV analysis consist of a volume fraction of each of the three components in each voxel. The results can be further used to calculate myelin water fraction (MWF), which is estimated as the percentage of the signal with T2 from the fast relaxation components (myelin water) to the total water content. The MWF is an important marker for white matter microstructure, especially myelin generation/degeneration, and thus a change in MWF has been associated with age-related neural tissue changes [15, 16], as well as neurodegenerative diseases such as Multiple Sclerosis [17] and Schizophrenia [18, 19].

In order to resolve multiple tissue components within one voxel, PV estimation methods employ multi-component signal models which are based on either contrast-weighted images or quantitative MRI scans. For the former scenario, weighted images with one or more contrasts are acquired and the PV is estimated based on regularized statistical models of image contrast variations [8, 20, 21]. Using quantitative MR to estimate PV has the benefit of having an additional time domain of the signal change that is characterized by one or more underlying tissue properties, such as T1 and/or T2. The PV effects can then be modeled by assuming that the acquired signal evolution is a mixture of multiple tissue components. For example, MWF estimation is based on multi-exponential T2 relaxation from a multiple spin-echo acquisition [19], and brain tissue segmentation is based on multi-exponential T1 relaxation from an inversion recovery Look-Locker acquisition [22] or based on multi-parametric mapping scans [10, 23]. The tissue fraction of each component is then estimated by interpolating between quantitative results [10], or by solving an inverse problem [22, 23].

MR Fingerprinting (MRF)[1] [24] is a quantitative MR method that provides new opportunities to analyze PV effects and identify multiple tissue components. First, MRF applies pseudorandomized acquisition patterns to generate signal evolutions that never stay at constant steady state and exhibit unique signal variations depending on multiple tissue properties. These two features help to provide more incoherent signals between different tissues, which could improve the ability of tissue separation. As an example, Figure 1 compares signals from a conventional T2 mapping method (left) and from MRF (right). Because signals from the conventional method all follow an exponential pattern, they are typically inseparable in the presence of noise. The mixed signal (green) with equal contributions from gray and white matter 'looks' the same as the signal from another, uniform tissue with a different T2 (red). In MRF, since signals do not follow such a simple evolution due to variable acquisition and multi-parametric sensitivity, the mixed signal is more likely to be distinct from other pure-tissue signals. Second, since the signal model is constructed based on Bloch equations, the effects from multiple tissue properties and confounding factors (B_0, slice profile and B_1 etc. [25-28]) can be accounted for. The PV results could thus be more robust and less dependent on system imperfections. Finally, we will show a few examples that pattern recognition based on a pre-defined dictionary could also make MRF-based PV analysis (PV-MRF) less sensitive to noise than conventional approaches based on inverse methods [23]. In the following sections, the theories and implementations of multiple PV-MRF methods will be introduced, followed by discussions of several emerging neuroimaging applications.

Partial volume signal model and conventional PV analysis

In both conventional quantitative MR and MRF, the acquired signal evolution such as shown in Figure 1B is modeled as a weighted sum of signals from a few known tissue components. Suppose the anatomy of interest contains m component tissues. Let $d_l \in C^{1 \times t}$ represent the MRF signal evolution for component tissue $1 \leq l \leq m$, where t is the number of time points acquired from an MRF scan or other T1 or T2 mapping experiment. We collect these m component signal evolutions in a sub-dictionary $D^{sub} \in C^{t \times m}$. The voxel signal evolution can be modeled as a weighted sum of the component species' signal evolutions:

$$s_i = \Sigma_{l=1}^{m} w_{i,l} d_l = D_{sub} W_i \quad (1)$$

where $w_{i,l}$ is the weight of tissue l in voxel i. For example, in normal brain tissues, we can model $m = 3$ to represent

GM, WM, and CSF. The number of components may be increased in cases of disease or complicated anatomy.

The signal of each component d_i can be simulated and is characterized by their tissue properties, such as T1, T2, and proton density (M_0). The values of these tissue properties can be either gathered from literature, group analysis, or estimated based on quantitative maps acquired from the same subject. The latter approach is more subject-specific and thus takes into account individual physiological variations. For example, multiple histograms of mapped relaxation times can be used to identify characteristic relaxation properties of the modeled tissues [22, 24]. Alternatively, *k*-means clustering can be used with MRF to identify voxels with similar relaxation properties based on T1 and T2 maps acquired from an MRF scan, yielding *k* clusters whose centroids represent characteristic {T1, T2} properties. The properties corresponding to those tissue clusters can then be selected as components in the PV model [23]. Note that the number of histograms or tissue clusters will affect T1 and T2 values of component tissues and thus affect the accuracy of the PV analysis.

After the representative tissue properties are determined and the signals from D_{sub} are simulated (by Bloch equations, for example), the partial volume, or tissue fraction, of each component within a voxel is estimated by solving this linear model. The Moore-Penrose pseudoinverse is commonly applied to compute the signal weights:

$$W_i = (D^H_{sub} D_{sub})^{-1}\, D^H_{sub} s_i \quad (2)$$

where the superscript H represents the Hermitian adjoint or complex transpose operator. The weights are then normalized such that the sum of the weights has unit magnitude, and the result can be interpreted as a tissue fraction.

Tissue segmentation and partial volume quantification with PV-MRF

Solving the above inverse problem requires high SNR, which is typically not acquired in MRF due to highly accelerated *k*-space sampling and thus severe aliasing artifacts. The results are further prone to errors when more tissue components are assumed. Since dictionary matching has been shown to have relatively high error tolerance, a new dictionary-based PV-MRF has been proposed and has been shown to reduce the effect of over-fitting errors [23]. PV-MRF therefore adopts the concept of MRF, by converting a least-squares fitting problem into a pattern matching problem, where the weights are identified by exhaustive search of a new dictionary that contains all possible combinations of component tissues. To this end, a weight table $\widetilde{W} \in R^{m\times h}$ that lists all possible weight combinations is first constructed, where h is the number of weight combinations. Next, a separate PV dictionary is constructed,

$$D_{pv} = D_{sub}\widetilde{W} \in C^{t\times h} \quad (3)$$

where each column of D_{pv} contains a mixed tissue signal evolution calculated from the weighted sum of the m modeled component tissues with a certain weight combination. Finally, tissue fractions are estimated by matching the acquired signal to all signals from the PV dictionary. The weight combination corresponding to the highest inner product are selected and converted into multiple tissue fraction maps.

Figure 2 compares tissue fraction maps estimated from MRF signals using the pseudoinverse (2A) and dictionary based (2B) PV-MRF methods. GM, WM, and CSF maps from five 2D slices for one subject scanned on a 3T MAGNETOM Prisma are shown. Sequence parameters for each of the 2D MRF scans are: field of view = 300 x 300 mm², voxel resolution = 1.2 x 1.2 x 5 mm³, TA = 31 seconds [29].

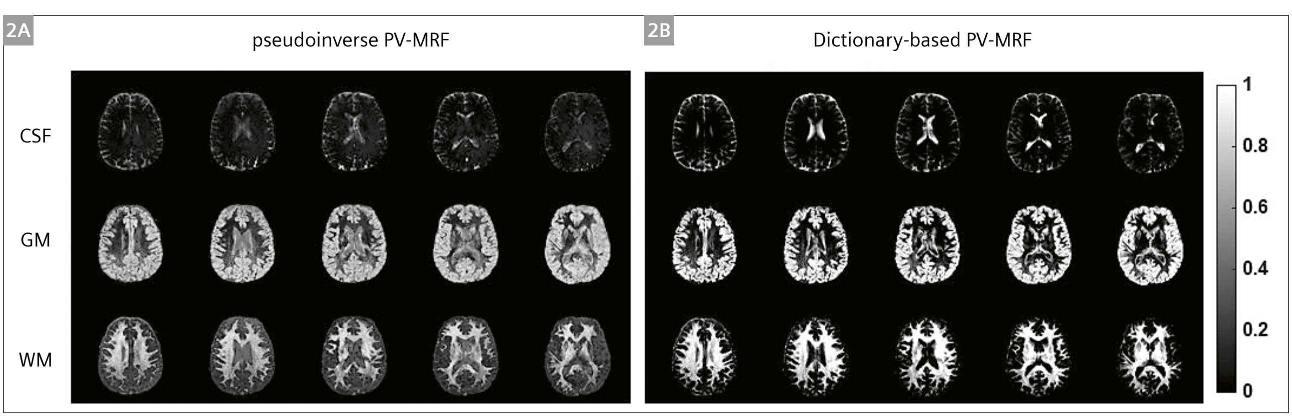

2 Comparison of partial volume estimation with MRF using conventional analysis by partial volume model inversion **(2A)** and dictionary-based PV-MRF **(2B)**. Dictionary matching is more robust to noise-like artifacts in MRF signals than the pseudoinverse calculation, allowing for better descrimination of tissues and more accurate estimation of tissue fractions [23].

PV-MRF can segment pure tissues, as well as visualize mixtures of GM and WM in deep gray matter structures. However, the PV fraction maps computed by pseudoinverse show residual CSF contributions in the GM and WM maps. The dictionary based PV-MRF maps exhibit better discrimination of pure tissues.

Figure 3 shows an example of all six 3D quantitative maps[1], including T1, T2, proton density, as well as GM, WM, and CSF fraction maps computed with a partial volume dictionary, acquired from a healthy volunteer scanned on a 3T MAGNETOM Prisma system. All maps are inherently co-registered because they are obtained from the same dataset. Sequence parameters for the 3D MRF scan are: field of view = 300 x 300 x 144 mm^3, voxel resolution = 1.2 x 1.2 x 1.2 mm^3 isotropic, TA = 12 minutes [30]. To compute tissue fraction maps using dictionary based PV-MRF, three tissue components, GM, WM, and CSF are assumed. *K*-means clustering of mapped T1 and T2 values with $k = 7$ is used to analyze tissue compositions based on the quantitative maps. Three clusters are then manually selected to identify the characteristic relaxation times of the modeled tissue components, which are subsequently used to construct D_{sub} and D_{pv}.

Bayesian model based PV-MRF

Most segmentation methods assume that the brain consists of only three tissue components (GM, WM, and CSF) and use this assumption to represent every voxel as a weighted sum of these three tissues. A limitation in this approach may be evident in cases of pathology, where a diseased or unhealthy tissue may not be composed of these three tissues, but may contain a different component not represented in the PV model. In this case, forcing a fixed model on the voxel signals will result in erroneous tissue fraction calculations and diseased tissue will not be properly characterized. To account for variations in both diseased and healthy tissues and relax the constraints of a fixed tissue model, a model was recently proposed using the Bayesian framework in which signal evolutions are fit to a larger dictionary with no prior assumption about how many or which tissue types may comprise the voxel signal [31]. In this method, the signal evolution is still modeled as a weighted sum of dictionary elements as in equation (1), however, a larger subset of tissue types is used with the assumption that many of the weights W_i should be zero, or in other words, that W_i should be a sparse vector,

$$s_i = DW_i \quad (4)$$

where D is the full MRF dictionary of simulated signal evolutions, and is of size $t \times n$, where $n >> t$. This is, however, an underdetermined problem, and solving using linear least-squares will result in a weight vector W_i which is not sparse. To achieve the desired result, a sparsity-promoting prior is placed on W_i, guiding the algorithm to fit the signal evolution to the dictionary using only a few significant entries to represent the signal. The result of applying this model to a voxel signal evolution is a distribution of dictionary entries and corresponding weights that best describe the characteristics of the signal, and a voxel result is a matrix containing the T1, T2 pairs and corresponding weight values of the most significantly contributing dictionary entries.

An example of this method applied to a 3D MRF acquisition in an epilepsy patient is shown in Figure 4. The scatter plot shows Bayesian MRF results from four pixels indicated from a T1 map, one containing pure white matter (red), one containing pure gray matter (blue), one containing a mixture of white matter and gray matter (green) and one containing an epileptic lesion (black). The key advantage of using this Bayesian method is that the lesion cluster is not forced to fit to a fixed tissue model,

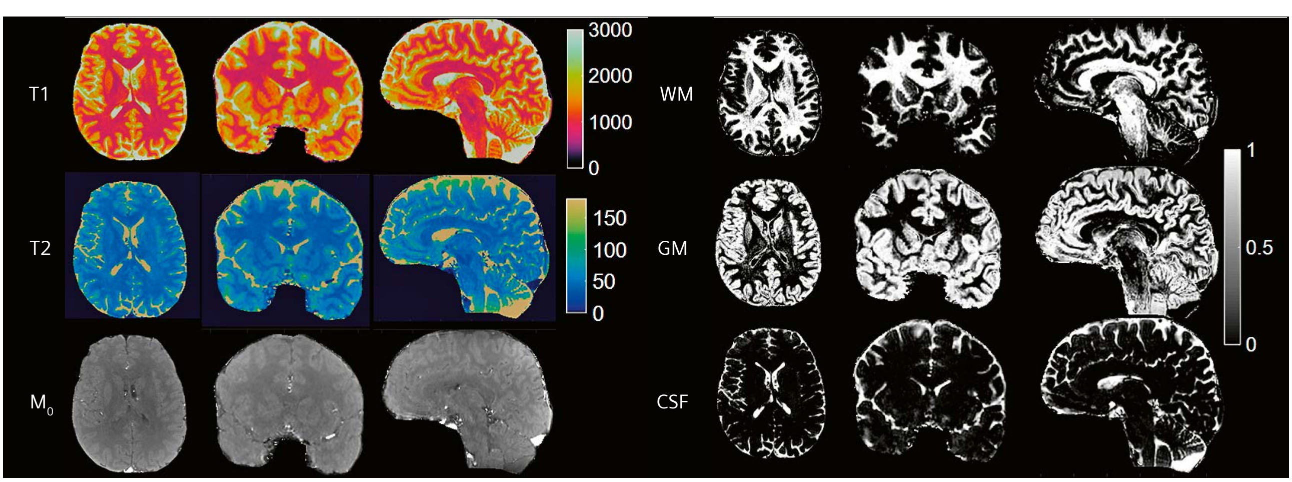

3 Six quantitative maps acquired from a single 3D MRF scan, providing co-registered 3D isotropic T1, T2, M_0 maps and GM, WM, CSF tissue fraction maps [30].

which may not include the relaxation properties of the lesion. The lesion is shown as a single cluster, which is different from those of two pure tissues (red and blue), while the PV pixel is identified by two separate green clusters, which are overlapped with the clusters from two pure tissues. This approach gives us a completely new tool to detect and characterize lesions.

The key feature of the Bayesian MRF method is that signal evolutions are not forced to fit a fixed model with predefined relaxation properties. However, this freedom results in distributions across voxels that may vary slightly, even within similar tissue structures. Summarizing the results is done most effectively by segmentation, using tissue fraction maps calculated from the Bayesian MRF results. To this end, voxel-wise results from the Bayesian method are combined across the full image or 3D volume and grouped using a Gaussian mixture model applied to the conglomerate T1, T2, and weight matrices. As there is no fixed tissue model in the Bayesian analysis, choosing a large enough number *K* of Gaussian distributions to represent the full range of possible tissue distributions is desirable. In a normal volunteer, one can assume fewer Gaussian distributions than in the case of disease. The mixture model allows for a probability to be associated to each point in T1, T2 space for each of the *K* Gaussian distributions. By using the Gaussian probability densities as a mask, tissue fraction maps can be calculated by multiplying the calculated weighted by the corresponding probabilities. These maps are normalized so that for each voxel, the fraction across each of the *k* classes is equal to one.

Potential clinical applications for neuroimaging

Epilepsy

Conventional MRI can be limited in its ability to recognize the existence and extent of subtle lesions, particularly focal cortical dysplasia (FCD). Up to 50% of potential epilepsy surgery candidates had a diagnosis

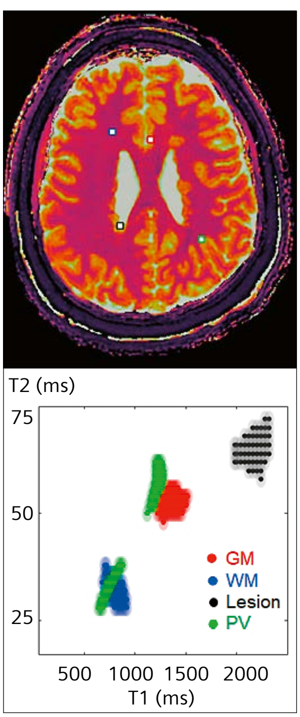

4 Example of Bayesian MRF results from a patient with right temporal-parietal epilepsy. Tissue compositions from four pixels located at healthy tissues (GM and WM), PV tissue at GM and WM boundary and epileptic nodule were analyzed. The results were able to separate lesion from healthy tissues, as well as PV effects.

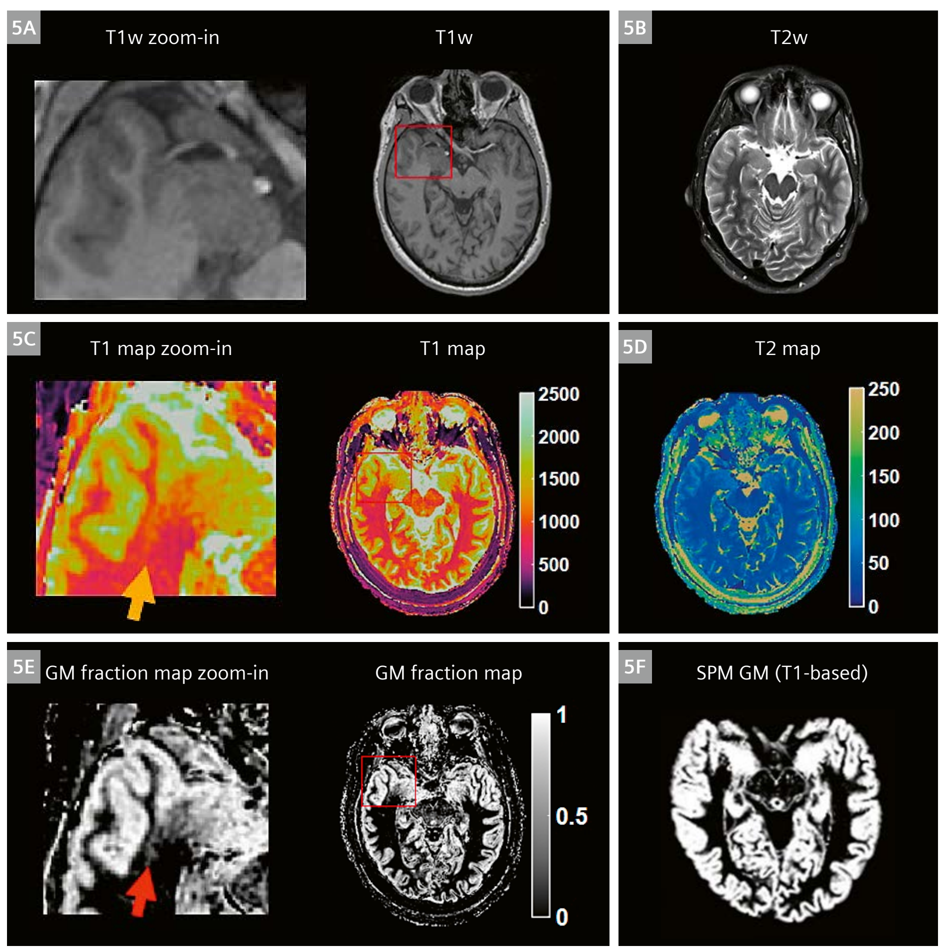

5 Patient with right temporal lobe epilepsy. **(5A, B)** T1w and T2w images from the clinical scans; **(5C, D)** T1 and T2 maps from the 3D MRF scan; **(5E, F)** GM fraction map from PV-MRF and T1w-based SPM segmentation. The potential epilepsy pathology (zoomed-in) identified from the MRF were not seen from the conventional MR scans [30].

of 'negative MRI', as there is no identifiable lesion to guide surgery. Our group recently demonstrated that 3D whole brain MRF and PV-MRF techniques can aid detection and characterization of lesions in epilepsy patients [30]. First, a fast and whole brain 3D MRF scan was applied to simultaneously quantify T1, T2, and proton density maps with 1.2 mm isotropic image resolution. The isotropic 3D maps allowed identification of lesions from multiple orientations and multiple tissue properties. Second, dictionary based PV-MRF [23] was applied to the same data to generate gray matter, white matter, and CSF maps. These maps could resolve multiple tissue components from a single voxel and additionally provide new contrasts along tissue boundaries. All available maps from a single scan are shown in Figure 3.

Figure 5 shows the MRF findings from a patient with right temporal lobe epilepsy. The clinical MRI showed that the right amygdala was enlarged with hyperintense FLAIR signal, with the right temporal lobe otherwise unremarkable by visual inspection (Figs. 5A, B). As shown in Figure 5C–E, MRF maps revealed a previously unseen signal abnormality 'tail' in addition to the amygdala hyperintensity. A subtle increase in the T1 value was seen on the T1 map (Fig. 5C) and increased gray matter fraction on the GM fraction map of the right superior temporal region (Fig. 5E), indicating potential abnormality. Figure 5E and 5F compare the GM fraction maps from MRF and from SPM segmentation of T1-weighted images. The GM map estimated from MRF not only identified the subtle tissue abnormality, but also showed wider variations of the gray matter fractions across the brain, which is believed to correspond to underlying cytostructure differences among different cortical regions. While this abnormality had no significant conspicuity on conventional MRI, the location of the abnormality was highly concordant with interictal and ictal EEG localization. Histopathology of the surgical specimen showed mild malformation of cortical development.

Figure 6 shows MRF and PV-MRF results from another patient with right temporo-parietal epilepsy, who had known bilateral periventricular heterotopias. As shown in Figure 6A and 6B, the nodules showed uniform signal intensity on clinical MRI scans as well as post-processing analysis using SPM segmentation of T1-weighted images. From Figure 6C and 6D, both the MRF T1 map and PV-MRF GM fraction maps showed increased values in the nodules at the right occipital horn. This distinct signal abnormality was not appreciable on the conventional MRI scans. The patient underwent invasive evaluation with stereotactic EEG (SEEG) targeting multiple brain regions. The nodules with abnormal signals shown by MRF and PV-MRF were consistent with the interictal SEEG findings and ictal onset of a typical seizure. Electrical stimulation of the electrodes at the right occipital horn produced habitual auras.

Brain development in early childhood

Chen et al. have recently applied MRF and dictionary based PV-MRF to characterize early brain developmental changes for healthy children from birth to five years old, who were enrolled in the UNC/UMN Baby Connectome Project [16]. In addition to T1 and T2 maps estimated from MRF scans, myelin water fraction (MWF) maps were estimated using dictionary based PV-MRF, by estimating tissue fractions from a three-compartment model including myelin water, intracellular/extracellular water, and free water. Representative T1, T2, and MWF maps from five subjects at different

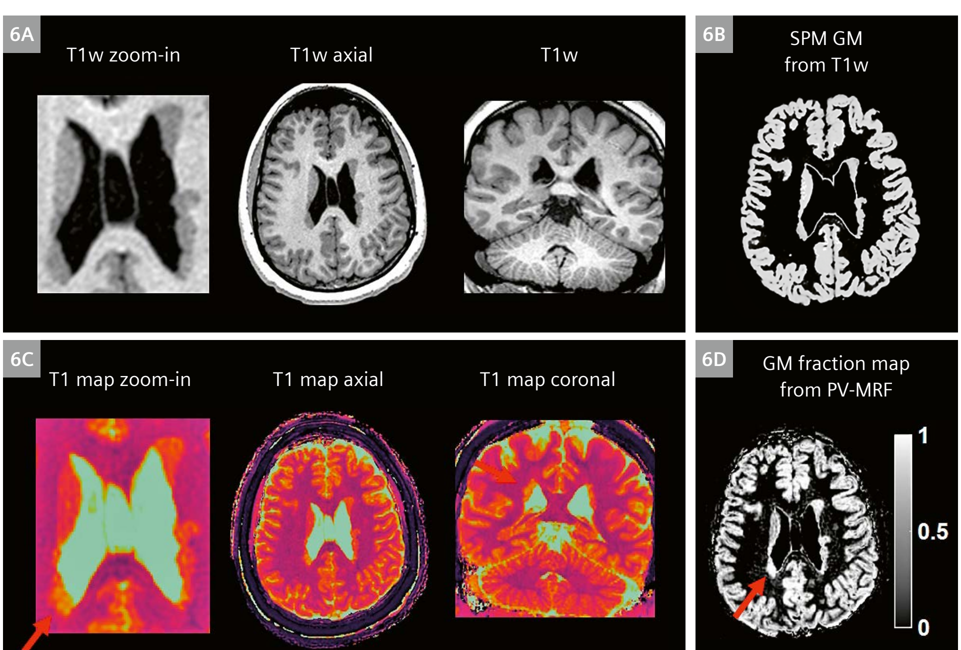

6 Patient with right temporo-parietal epilepsy. MRF was able to differentiate the active/epileptogenic heterotopic nodules from the non-active/non-epileptogenic ones **(6A)** Axial and coronal T1w image from the clinical scan. **(6B)** Corresponding T1 map from MRF. **(6C)** GM fraction map from T1w-based SPM segmentation. **(6D)** GM fraction map from PV-MRF [30].

ages are shown in Figure 7. Both T1 and T2 values decrease while MWF increases with age. Based on the results from 28 children, R1 (1/T1) and R2 (1/T2) showed a marked increase until approximately 20 months of age, followed by a slower increase for all WM regions. The MWF remained at a negligible level until about 6 months of age and gradually increased afterwards. In addition, significant differences in R1 and MWF trajectories were observed across different white matter region, and the spatial pattern for myelination during early brain development matches well to the previous findings obtained from post-mortem brain tissues [32].

Brain tumors

Depending on the stage, cancers originating or metastasized in the brain can be heterogeneous, containing regions of solid cellular neoplasms, edema, inflammation, cysts, and necrosis. However, conventional approaches using pseudoinverse calculations to invert partial volume models result in less accurate tissue fraction estimations as the PV model complexity increases. Moreover, these complex PV models can be difficult to establish, since unlike normal tissue segmentation or microstructure evaluation, the relaxation properties of heterogeneous tissue compartments cannot be easily determined for each subject or obtained from the literature. PV analysis in tumors therefore requires careful construction of a comprehensive partial volume model, which encompasses multiple types of diseased tissue.

In heterogeneous tissues such as the region in and around the brain tumor, pure tissues may not occupy enough voxels for *k*-means clustering of mapped T1 and T2 values to identify unique tissues. Bayesian MRF analysis provides particular value in these scenarios. Figure 8 shows the results from three different slices of a patient diagnosed with a glioblastoma brain tumor (GBM). The patient gave written consent and was scanned with 3D-MRF FISP acquisition with image resolution of 1.2 x 1.2 x 3 mm^3. A Gaussian mixture model was applied to the Bayesian results, with $K = 14$ Gaussian distributions found. Shown in Figure 8 are the weight maps from 8 of these distributions, corresponding to (from left to right) white matter, two gray matter classes, CSF, and two clusters related to the tumor pathology. Remaining maps from the other eight tissue distributions correspond to other tissues, such as fat and bone surrounding the brain, or may have very small weights in comparison to the six shown.

Bayesian MRF and dictionary-based PV-MRF work hand-in-hand. In place of or in addition to using *k*-means clustering of T1 and T2 times, Bayesian MRF can help establish the relaxation times of healthy and diseased tissues in and around the brain tumor. This information can

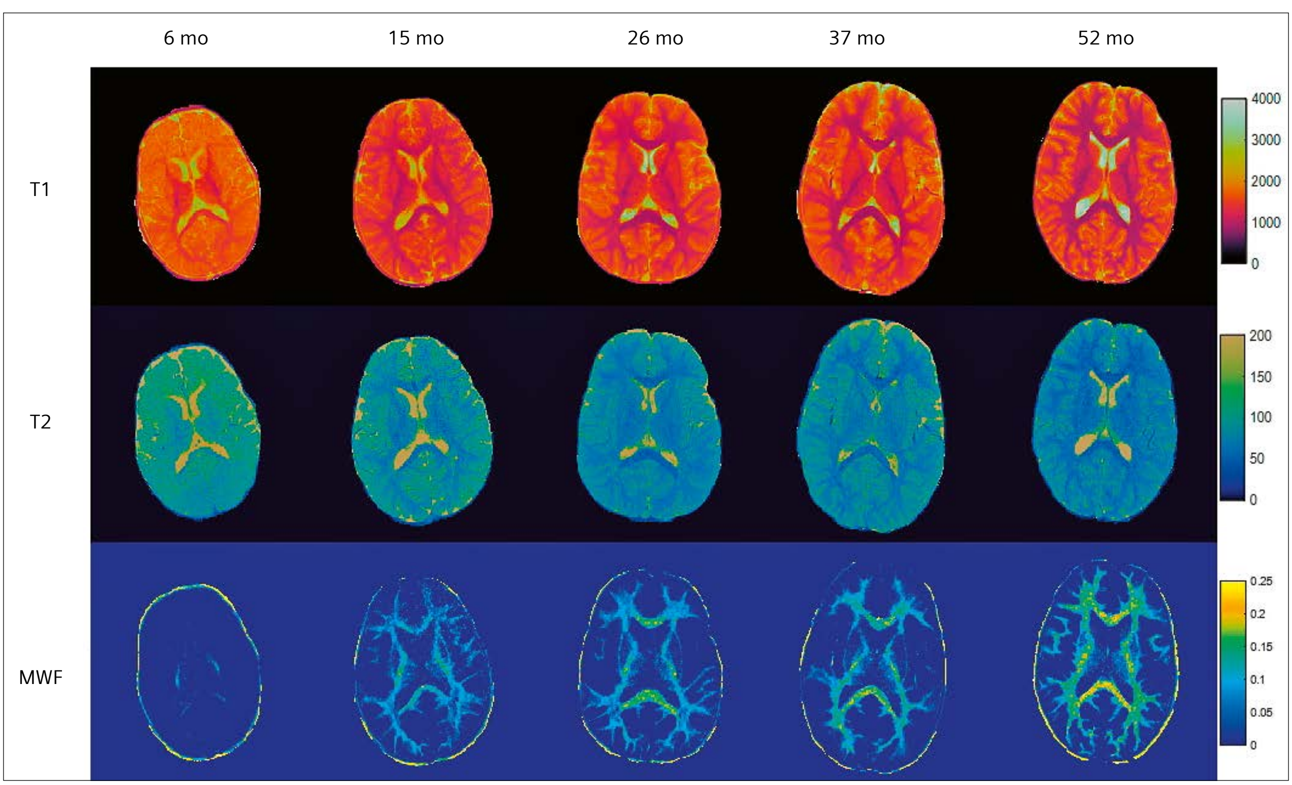

7 Representative T1, T2 and MWF maps from five subjects at different ages. Similar slice location that covers the genu and splenium of the corpus callosum was selected. Both T1 and T2 decrease while MWF increases with age [16].

then be used to construct D_{sub} and D_{pv} for dictionary-based PV-MRF for segmentation and estimation of diseased tissue fractions. Figure 9 shows an example of tissue segmentation and partial volume estimation using dictionary-based PV-MRF [23] in a patient with a small-cell lung cancer metastasis in the brain, scanned with 3D MRF on a 3T MAGNETOM Prisma system. Clinically-acquired FLAIR and contrast-enhanced T1-weighted images show an enhancing tumor with cystic and necrotic components, and surrounding edema. MRF provides 3D maps of T1, T2, and M_0, from which distinct relaxation times for normal appearing brain tissues (fat, GM, WM, CSF) and diseased tissues could be identified by *k*-means clustering and confirmed by Bayesian MRF analysis in these regions. An expanded partial volume dictionary containing all possible combinations of six tissue components allows for segmentation and volume fraction estimation of normal as well as tumor tissues, including solid enhancing components, cystic components, and the surrounding edema. Note that dictionary-based PV-MRF provides quantitative maps of tissue volume

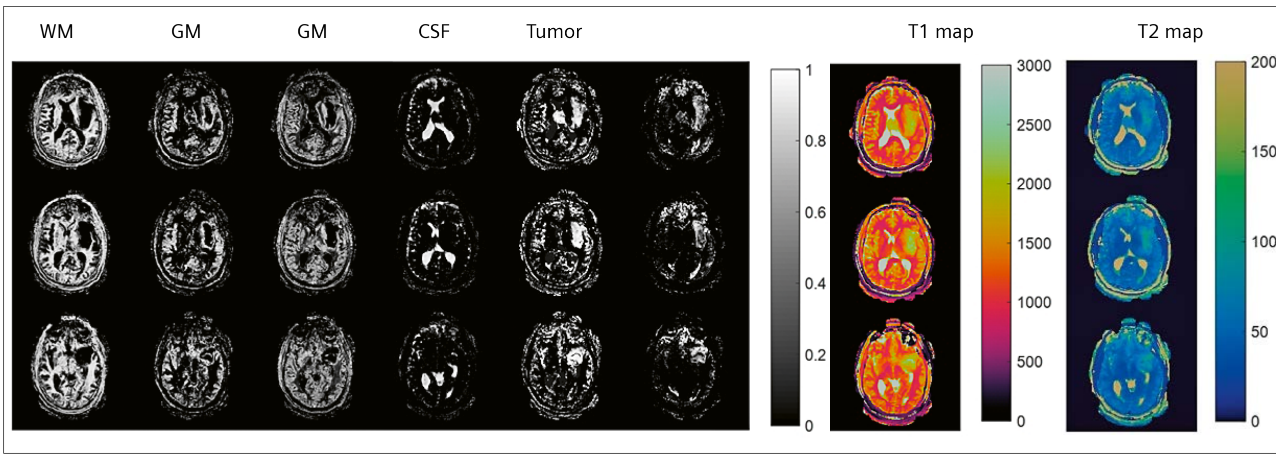

8 Six partial volume maps are displayed on the left for three different slices in a patient with glioblastoma. Since the method makes no assumptions about which type of tissues are present, the resulting cluster labels are assigned as a final step. From left to right are weight maps for white matter, gray matter, a mix of gray matter and wm/gm partial volume, csf, solid tumor, and some peritumoral white matter. Note there are two lesions. On the far right are the corresponding T1 and T2 maps for each slice [33].

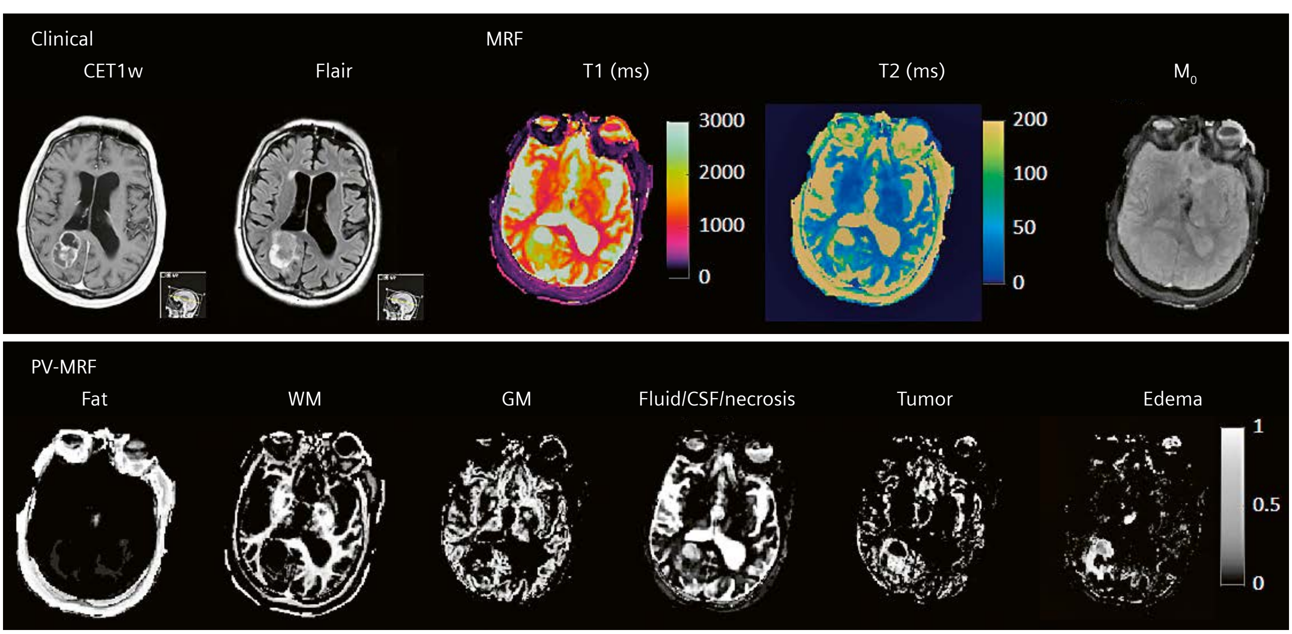

9 Segmentation of a small-cell lung cancer metastasis in the brain using dictionary-based PV-MRF and 3D MRF acquisition. Dictionary matching enables the use of expanded multi-component models and segmentation of more tissue types compared to conventional partial volume analysis [23].

fractions, as shown in Figure 9 [23], whereas the Bayesian MRF visualization illustrated in Figure 8 visualizes weighted probabilities that each voxel corresponds to the particular tissue class.

Improved synthetic imaging

It is sometimes the case that certain contrast weightings are unavailable for diagnosis, due to poor patient compliance or scan time limitations. Quantitative mapping of underlying tissue MR properties with methods like MRF opens the possibility for synthetic MRI. Rather than scanning the patient again to acquire new images with the desired contrast, these images can be synthesized or calculated off-line by applying known equations to the underlying tissue properties T1, T2, and M_0, mapped with quantitative MRI. With this approach, image contrast can be optimized for discrimination of lesions without the associated lengthy scan time. Synthetic imaging can also be a useful aid in the transition between interpreting multiple weighted-contrast images, which is currently standard clinical practice, and quantitative maps.

While typical T1- and T2-weighted images are straightforward to calculate, synthetic MRI of widely used sophisticated contrast weightings such as fluid attenuated inversion recovery (FLAIR) still pose a challenge due to partial volume effects. This challenge is illustrated in Figure 10. In a FLAIR sequence, the image is acquired when the magnetization of the fluid is nulled and does not contribute to the voxel signal. However, in voxels containing partial volumes mapped T1 and T2 values will be influenced by the long relaxation times associated with fluids. A synthetic FLAIR image calculated from mapped MRF relaxation times therefore will have poor contrast in the sulci, where partial volumes of fluid contaminate the mapped relaxation times.

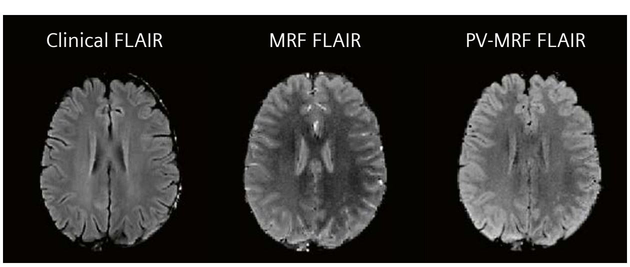

10 Improved synthetic MRI with PV-MRF. In a fluid attenuated inversion recovery (FLAIR) sequence, the magnetization of fluid is nulled and does not contribute signal in the acquired image (left). Synthetic FLAIR images calculated from MRF parameter maps exhibit distorted contrast in regions containing partial volumes of CSF such as the sulci, since the relaxation times in these voxels reflect contributions from fluid. Estimation of fluid fractions by PV-MRF and removal of the fractional fluid contribution to the voxel signal evolution allows for more accurate estimation of relaxation times in these partial volume voxels, enabling improved contrast in the synthetic FLAIR images [34].

Here again the uniqueness of MRF signal evolutions provides an advantage: not only can fluid partial volumes in each voxel be quantified with PV-MRF, the corresponding contribution of fluid signals can also be subtracted from the measured voxel signal. The remaining voxel signal, reflecting the signal evolutions of the remaining non-fluid tissues, can be matched to the MRF dictionary again and the resulting T1 and T2 maps can be used to calculate the synthetic FLAIR image. This approach improves the contrast of the synthetic FLAIR by effectively "nulling" the partial volume contribution of fluid in each voxel in post-processing [34].

Conclusion

MRF allows for fast, robust, simultaneous quantification of multiple tissue properties. Moreover, the unique signal shapes generated by the pseudorandom MRF sequence allow for additional insight into the multi-component contributions to the voxel signal evolution. Using dictionary-based PV-MRF, partial volumes of healthy and diseased tissues and microstructures can be robustly segmented and estimated. Properties of component tissues, including diseased tissues in tumors, can be determined without prior knowledge by *k*-means clustering of quantitative MRF results or through sophisticated Bayesian analysis of sub-voxel compositions. In combination, MRF, Bayesian MRF, and PV-MRF can provide new, clinically-relevant information about subtle tissue changes which may not be apparent on conventional weighted MR images.

[1] *Work in progress: the application is currently under development and is not for sale in the U.S. and in other countries. Its future availability cannot be ensured.*

References

1 Warfield, S. K. et al. Automated segmentation of multiple sclerosis lesion subtypes with multichannel MRI. Neuroimage 32, 1205–1215 (2006).
2 Pundik, S., Scoco, A., Skelly, M., McCabe, J. P. & Daly, J. J. Greater Cortical Thickness Is Associated With Enhanced Sensory Function After Arm Rehabilitation in Chronic Stroke. Neurorehabil. Neural Repair (2018).
3 Busch, V., Gaser, C. & Busch, V. Changes in grey matter induced by training Newly honed juggling skills show up as a transient feature on a brain-imaging scan. Nature 427, 311–312 (2004).
4 Barnes, J., Ourselin, S. & Fox, N. C. Clinical application of measurement of hippocampal atrophy in degenerative dementias. Hippocampus 19, 510–516 (2009).
5 Adler, S. et al. Towards in vivo focal cortical dysplasia phenotyping using quantitative MRI. NeuroImage Clin. 15, 95–105 (2017).
6 Hong, S. J., Bernhardt, B. C., Schrader, D. S., Bernasconi, N. & Bernasconi, A. Whole-brain MRI phenotyping in dysplasia-related frontal lobe epilepsy. Neurology 86, 643–650 (2016).

7 Li, N. et al. Optimization and comparative evaluation of nonlinear deformation algorithms for atlas-based segmentation of DBS target nuclei. Neuroimage 184, 586–598 (2018).
8 Choi, H. S., Haynor, D. R. & Kim, Y. Partial volume tissue classification of multichannel magnetic resonance images-a mixel model. IEEE Trans. Med. Imaging 10, 395–407 (1991).
9 Alfano, B. et al. Unsupervised, automated segmentation of the normal brain using a multispectral relaxometric magnetic resonance approach. Magn. Reson. Med. 37, 84–93 (1997).
10 West, J., Warntjes, J. B. M. & Lundberg, P. Novel whole brain segmentation and volume estimation using quantitative MRI. Eur. Radiol. 22, 998–1007 (2012).
11 Reeder, S. B., Cruite, I., Hamilton, G. & Sirlin, C. B. Quantitative Assessment of Liver Fat with Magnetic Resonance Imaging and Spectroscopy. J. Magn. Reson. Imaging (2011).
12 Huppertz, H. J. et al. Voxel-based 3D MRI analysis helps to detect subtle forms of subcortical band heterotopia. Epilepsia 49, 772–785 (2008).
13 Wang, I. & Alexopoulos, A. MRI postprocessing in presurgical evaluation. Curr. Opin. Neurol. 29, 168–174 (2016).
14 Whittall, K. P. et al. In Vivo Measurement of T2 Distributions and Water Contents in Normal Human Brain. Magn. Reson. Med. 37, 34–43 (1997).
15 Guttmann, C. R. G. et al. White matter changes with normal aging. Neurology 42, 5–5 (1998).
16 Chen, Y. et al. MR Fingerprinting enables quantitative measures of brain tissue relaxation times and myelin water fraction in early brain development. Neuroimage 186, 782–793 (2019). 186, 782-793 (2019).
17 Monohan, E. et al. Measuring longitudinal myelin water fraction in new multiple sclerosis lesions. NeuroImage Clin. 9, 369–375 (2015).
18 Flynn, S. W. et al. Abnormalities of myelination in schizophrenia detected in vivo with MRI and post-mortem with analysis of oligodendrocyte proteins. Mol. Psychiatry 8, 811–820 (2003).
19 Honer, W. G. et al. 48 echo T2 myelin imaging of white matter in first-episode schizophrenia: Evidence for aberrant myelination. NeuroImage Clin. 6, 408–414 (2014).
20 Shattuck, D. W., Sandor-Leahy, S. R., Schaper, K. A., Rottenberg, D. A. & Leahy, R. M. Magnetic Resonance Image Tissue Classification Using a Partial Volume Model. Neuroimage 13, 856–876 (2001).
21 Bonar, D. C., Schaper, K. A., Anderson, J. R., Rottenberg, D. A. & Strother, S. C. Graphical analysis of MR feature space for measurement of CSF, gray-matter, and white-matter volumes. J. Comput. Assist. Tomogr. 17, 461–70
22 Shin, W. et al. Automated brain tissue segmentation based on fractional signal mapping from inversion recovery Look-Locker acquisition. Neuroimage 52, 1347–1354 (2010).
23 Deshmane, A. et al. Partial volume mapping using magnetic resonance fingerprinting. NMR Biomed. (2019). doi:10.1002/nbm.4082
24 Liao, C. et al. Detection of Lesions in Mesial Temporal Lobe Epilepsy by Using MR Fingerprinting. Radiology 288, 804–812 (2018).
25 Ma, D. et al. Slice profile and B1 corrections in 2D magnetic resonance fingerprinting. Magn. Reson. Med. 78, 1781–1789 (2017).
26 Buonincontri, G. & Sawiak, S. J. MR fingerprinting with simultaneous B1 estimation. Magn. Reson. Med. 76, 1127–1135 (2016).
27 Cloos, M. A. et al. Multiparametric imaging with heterogeneous radiofrequency field: Additional material. Nat. Commun. 7, (2016).
28 Körzdörfer, G. et al. Magnetic resonance field fingerprinting. Magn. Reson. Med. 81, 2347–2359 (2019).
29 Jiang, Y., Ma, D., Seiberlich, N., Gulani, V. & Griswold, M. a. MR fingerprinting using fast imaging with steady state precession (FISP) with spiral readout. Magn. Reson. Med. (2014).
30 Ma, D. et al. Development of high-resolution 3D MR fingerprinting for detection and characterization of epileptic lesions. J. Magn. Reson. Imaging 1–14 (2018). doi:10.1002/jmri.26319
31 McGivney, D. et al. Bayesian estimation of multicomponent relaxation parameters in magnetic resonance fingerprinting. Magn. Reson. Med. 80, 159-170 (2018).
32 Hertz-Pannier, L. et al. The early development of brain white matter: A review of imaging studies in fetuses, newborns, and infants. Neuroscience 276, 48–71 (2014).
33 McGivney D., Jiang Y, Ma D, Badve C., Gulani V., Griswold M. Segmentation of brain tissues using a Bayesian estimation of multicomponent relaxation values in magnetic resonance fingerprinting. Proc. Intl. Soc. Mag. Reson. Med. 26 (2018) No. 1022.
34 Deshmane, A. et al. Accurate Synthetic FLAIR Images Using Partial Volume Corrected MR Fingerprinting. in Proc.Intl.Soc.Mag.Reson.Med (2016).

Contact

Dan Ma
Department of Radiology
Case Western Reserve University,
School of Medicine
11100 Euclid Ave
Cleveland, OH 44106
USA
Tel.: +1 216-844-3916
dxm302@case.edu